The scaled boundary finite element method for plate bending problems

Rolf Dieringer[1], **Jochen Hebel**[2], **Wilfried Becker**[3]

[1] *Chair of Structural Mechanics, TU Darmstadt*
Hochschulstr. 1, 64289 Darmstadt, Germany
e-mail: dieringer@fsm.tu-darmstadt.de

[2] *Chair of Solid Mechanics, TU Darmstadt*
Hochschulstr. 1, 64289 Darmstadt, Germany
e-mail: hebel@mechanik.tu-darmstadt.de

[3] *Chair of Structural Mechanics, TU Darmstadt*
Hochschulstr. 1, 64289 Darmstadt, Germany
e-mail: becker@fsm.tu-darmstadt.de

Abstract

The scaled boundary finite element method is extended to the static analysis of thin plates in the framework of Kirchhoff's plate theory. The governing equations are transformed into scaled boundary coordinates. Applying a discrete form of the Kantorovich reduction method, a system of ordinary differential equations for the unknown displacement functions is obtained, which is solved in a closed-form analytical manner. Element stiffness matrices for bounded and unbounded domains are computed, using appropriate subsets of the solution. Numerical examples show the accuracy and efficiency of the scaled boundary finite element method applied to plate bending problems.

Keywords: structural mechanics, plates, numerical analysis, finite element methods

1. Introduction

The scaled boundary finite element method (SBFEM) is a semi-analytical analysis technique, combining advantages of the finite element method (FEM) and the boundary element method, whereas in the SBFEM no fundamental solution is needed. The method was first developed by Wolf and Song for the computation of the dynamic stiffness of unbounded media (Refs. [1], [2], [3]) and for elastostatics via the virtual work balance by Deeks and Wolf (Ref. [4]). Essential to the method is the mapping of a domain's boundary to a scaling centre. This is achieved introducing the so-called scaled boundary coordinate system. Then, the governing equations can be handled in scaling direction in a strong form, while working in the other direction, which forms the boundary, in a weak form using a finite element approximation. If linear elastic material behaviour is assumed, the strong form leads to a set of differential equations, which can be solved in a closed-form analytical manner via the corresponding eigenvalue problem. Additionally, a boundary stiffness matrix $\mathbf{K}$ is obtained by the solution procedure, relating the nodal displacements and the nodal forces and moments on the boundary. Finally, the displacements within the domain can be calculated, knowing the displacements at the boundary. The displacement field is expanded in form of a series. This characteristic of the expansion of the displacement field enables the robust calculation of intensities and exponents of singular fields, making the SBFEM especially useful for the analysis of cracked and notched structures. Song used this characteristic feature of the SBFEM for the evaluation of power-logarithmic singularities at cracks and multi-material corners (Ref. [5]). Furthermore, Song and Vrcelj applied the SBFEM for the calculation of dynamic stress intensity factors (Ref. [6]). Lindemann and Becker used the method for the assessment of stress concentrations at holes in composites (Ref. [7]). Finally, Artel and Becker expanded the method for the analysis of free-edge stresses in multi-material laminates (Ref. [8]). Even though the SBFEM has been applied to many problems of continuum mechanics with great success, there is up to now no successful application to plate bending problems. This study provides the employment of the SBFEM to plate bending problems. The derivation of the scaled boundary finite element equation in displacements for plate bending problems, as shown in this paper, is performed, using the virtual work principle. Numerical examples demonstrate the accuracy and efficiency of the method's application to plate bending problems.

2. Virtual work equivalence for Kirchhoff plates

For thin plates with vanishing transversal shear deformations, the kinematical assumption of Kirchhoff ($\nabla w + \boldsymbol{\phi} = 0$) holds. Neglecting body loads, the virtual work equivalence is given by

$$\int_{\Omega} \left(\boldsymbol{\mathcal{L}}\boldsymbol{\nabla}\delta w\right)^T \mathbf{D}_D \left(\boldsymbol{\mathcal{L}}\boldsymbol{\nabla} w\right) d\Omega = \int_{\Gamma_n} \delta\phi_n \bar{M}_n d\Gamma + \int_{\Gamma_t} \delta\phi_s \bar{M}_{ns} d\Gamma + \int_{\Gamma_s} \delta w \bar{S}_n d\Gamma, \qquad (1)$$

where Ω denotes the area of the plate's reference surface, $\mathbf{D}_D$ is the plate stiffness. $\boldsymbol{\mathcal{L}}$ and $\boldsymbol{\nabla}$ describe differential operators. The out-of-plane displacements w and the rotations $\boldsymbol{\phi}$ are kinematical variables. $\bar{M}_n, \bar{M}_{ns}, \bar{S}_n$ are traction resultants at the corresponding parts of the boundary Γ_n, Γ_t and Γ_s.

3. Scaled boundary finite element discretisation

3.1. Approximation of geometry

Essential to the SBFEM is the scaling of a domain relative to a scaling centre $S(x_0, y_0)$, selected within the domain. The normalised radial coordinate ξ ($\xi_i \leq \xi \leq \xi_e$) runs from the scaling centre ($\xi = 0$) to the boundary ($\xi = 1$), the other circum-

ferential coordinate η describes a length around the boundary ($0 \leq \eta \leq \Gamma$).

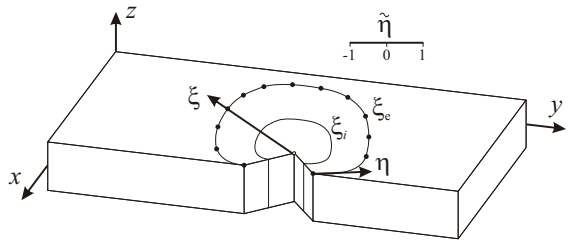

Figure 1: Definition of the scaled boundary coordinate system.

The scaled boundary and the Cartesian coordinate system are related using the transformation

$$\mathbf{x} = \mathbf{x}_0 + \xi\hat{\mathbf{N}}(\tilde{\eta})\mathbf{x}_s = \mathbf{x}_0 + \xi \begin{bmatrix} \hat{\mathbf{n}}^x(\tilde{\eta}) \\ \hat{\mathbf{n}}^y(\tilde{\eta}) \end{bmatrix} \mathbf{x}_s. \tag{2}$$

Linear functions of the local boundary coordinate $\tilde{\eta}$ are applied for the geometry shape functions $\hat{\mathbf{N}}(\tilde{\eta})$. The scaling centre is located at $\mathbf{x}_0$, the coordinates of the outer boundary are related to the scaling centre using $\mathbf{x}_s$. Derivatives in scaled boundary coordinates are related to derivatives in the Cartesian coordinate system using the Jacobi matrix

$$\begin{bmatrix} \frac{\partial}{\partial\xi} \\ \frac{\partial}{\partial\eta} \end{bmatrix} = \mathbf{J} \begin{bmatrix} \frac{\partial}{\partial x} \\ \frac{\partial}{\partial y} \end{bmatrix} = \begin{bmatrix} \hat{\mathbf{n}}^x\mathbf{x}_s & \hat{\mathbf{n}}^y\mathbf{x}_s \\ \xi\hat{\mathbf{n}}^x_{,\eta}\mathbf{x}_s & \xi\hat{\mathbf{n}}^y_{,\eta}\mathbf{x}_s \end{bmatrix} \begin{bmatrix} \frac{\partial}{\partial x} \\ \frac{\partial}{\partial y} \end{bmatrix}. \tag{3}$$

Inverting yields the following relation:

$$\begin{bmatrix} \frac{\partial}{\partial x} \\ \frac{\partial}{\partial y} \end{bmatrix} = \frac{1}{\det\mathbf{J}} \begin{bmatrix} \xi\hat{\mathbf{n}}^y_{,\eta}\mathbf{x}_s & -\hat{\mathbf{n}}^y\mathbf{x}_s \\ -\xi\hat{\mathbf{n}}^x_{,\eta}\mathbf{x}_s & \hat{\mathbf{n}}^x\mathbf{x}_s \end{bmatrix} \begin{bmatrix} \frac{\partial}{\partial\xi} \\ \frac{\partial}{\partial\eta} \end{bmatrix}$$

$$= \begin{bmatrix} j^*_{11} & j^*_{12} \\ j^*_{21} & j^*_{22} \end{bmatrix} \begin{bmatrix} \frac{\partial}{\partial\xi} \\ \frac{1}{\xi}\frac{\partial}{\partial\eta} \end{bmatrix}, \tag{4}$$

where the determinant of the Jacobian is given by

$$\det\mathbf{J} = \xi\det\mathbf{J}^* = \xi\left(\hat{\mathbf{n}}^x\mathbf{x}_s\hat{\mathbf{n}}^y_{,\eta}\mathbf{x}_s - \hat{\mathbf{n}}^y\mathbf{x}_s\hat{\mathbf{n}}^x_{,\eta}\mathbf{x}_s\right). \tag{5}$$

The differential operator $\boldsymbol{\mathcal{L}}$, relating the strains and the displacement, can be rewritten in the following way:

$$\boldsymbol{\mathcal{L}} = \begin{bmatrix} \frac{\partial}{\partial x} & 0 \\ 0 & \frac{\partial}{\partial y} \\ \frac{\partial}{\partial y} & \frac{\partial}{\partial x} \end{bmatrix} = \hat{\mathbf{B}}_1(\tilde{\eta})\frac{\partial}{\partial\xi} + \frac{1}{\xi}\hat{\mathbf{B}}_2(\tilde{\eta})\frac{\partial}{\partial\eta}$$

$$= \begin{bmatrix} j^*_{11} & 0 \\ 0 & j^*_{21} \\ j^*_{21} & j^*_{11} \end{bmatrix} \frac{\partial}{\partial\xi} + \frac{1}{\xi} \begin{bmatrix} j^*_{12} & 0 \\ 0 & j^*_{22} \\ j^*_{22} & j^*_{12} \end{bmatrix} \frac{\partial}{\partial\eta}. \tag{6}$$

The nabla operator can be posed in a similar form:

$$\boldsymbol{\nabla} = \hat{\mathbf{B}}_3(\tilde{\eta})\frac{\partial}{\partial\xi} + \frac{1}{\xi}\hat{\mathbf{B}}_4(\tilde{\eta})\frac{\partial}{\partial\eta}$$

$$= \begin{bmatrix} j^*_{11} \\ j^*_{21} \end{bmatrix} \frac{\partial}{\partial\xi} + \frac{1}{\xi} \begin{bmatrix} j^*_{12} \\ j^*_{22} \end{bmatrix} \frac{\partial}{\partial\eta}. \tag{7}$$

The matrices $\hat{\mathbf{B}}(\tilde{\eta})$ contain only components of the inverse Jacobian, which is evaluated at the boundary ($\xi_e = 1$) in an element-wise manner. For thin plates, shear deformations are neglected according to the Kirchhoff assumption. Then, the strain-displacement relations can be described using the curvatures of the midplane of the plate. Therefore, the derivatives of second order have to be formulated in scaled boundary coordinates also:

$$\boldsymbol{\mathcal{L}}\boldsymbol{\nabla} = \frac{1}{\xi}\hat{\mathbf{B}}_5(\tilde{\eta})\frac{\partial}{\partial\xi} + \frac{1}{\xi^2}\hat{\mathbf{B}}_6(\tilde{\eta})\frac{\partial}{\partial\eta} + \hat{\mathbf{B}}_7(\tilde{\eta})\frac{\partial^2}{\partial\xi^2} + \frac{1}{\xi^2}\hat{\mathbf{B}}_8(\tilde{\eta})\frac{\partial^2}{\partial\eta^2} + \frac{1}{\xi}\hat{\mathbf{B}}_9(\tilde{\eta})\frac{\partial^2}{\partial\eta\partial\xi}. \tag{8}$$

If the geometry of the domain is linearly interpolated, $\hat{\mathbf{B}}_5(\tilde{\eta}) = 0$ holds. For the other matrices, the following relations are given:

$$\hat{\mathbf{B}}_6(\tilde{\eta}) = \begin{bmatrix} -2j^*_{11}j^*_{12} \\ -2j^*_{21}j^*_{22} \\ -2(j^*_{11}j^*_{22} + j^*_{12}j^*_{21}) \end{bmatrix}; \quad \hat{\mathbf{B}}_7(\tilde{\eta}) = \begin{bmatrix} j^{*2}_{11} \\ j^{*2}_{21} \\ 2j^*_{11}j^*_{21} \end{bmatrix};$$

$$\hat{\mathbf{B}}_9(\tilde{\eta}) = \begin{bmatrix} 2j^*_{11}j^*_{12} \\ 2j^*_{21}j^*_{22} \\ 2(j^*_{11}j^*_{22} + j^*_{12}j^*_{21}) \end{bmatrix}; \quad \hat{\mathbf{B}}_8(\tilde{\eta}) = \begin{bmatrix} j^{*2}_{12} \\ j^{*2}_{22} \\ 2j^*_{12}j^*_{22} \end{bmatrix}. \tag{9}$$

3.2. Derivation of the scaled boundary finite element equation for straight discretised boundaries

The presence of second derivatives in the virtual work balance indicates, that for the formulation of thin Kirchhoff plates C_1 continuity of the displacement shape functions must be ensured. It is difficult, to achieve these continuity requirements for standard FEM formulations. Furthermore, it is impossible to specify simple polynomials for shape functions ensuring full compatibility for standard FEM discretisations, when only w and its slopes are prescribed at the corner nodes (Ref. [9]). C_1 continuity requirements pose also difficulties, using the SBFEM discretisation, but these difficulties are less than those, which arise in standard finite element formulations for plate bending elements. As mentioned above, a key feature of the SBFEM is, that only the boundary of a domain needs to be discretised. The displacements are approximated, using a separable product form:

$$w(\xi,\eta) = \mathbf{N}_w(\eta)\mathbf{w}_h(\xi). \tag{10}$$

Now, a straight discretised boundary in the SBFEM is regarded, as pictured in Fig 2. Each element is described using a mapping of the element's boundary with respect to a scaling centre. If along adjacent element boundaries unknown displacement functions $w(\xi)$ and $\frac{\partial w}{\partial\eta}(\xi)$ are adopted, the use of Hermitian polynomials as displacement shape functions is sufficient, to ensure C_1 continuity all over the domain for the regarded case.

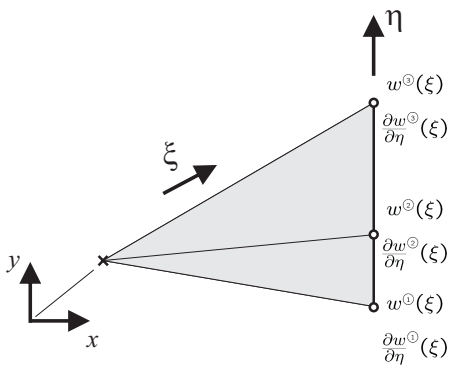

Figure 2: Scaled boundary discretisation.

The approach conforms largely to the application of Hermitian polynomials of cubic order, which are used as displacement shape functions for Euler-Bernoulli beams in standard FEM formulations (Ref. [9]). So, the displacement field within an element is approximated using the following relation:

$$w(\xi,\eta) = \begin{bmatrix} \frac{1}{4}(2-3\tilde{\eta}+\tilde{\eta}^3) \\ \frac{l_e}{8}(1-\tilde{\eta}-\tilde{\eta}^2+\tilde{\eta}^3) \\ \frac{1}{4}(2+3\tilde{\eta}-\tilde{\eta}^3) \\ \frac{l_e}{8}(-1-\tilde{\eta}+\tilde{\eta}^2+\tilde{\eta}^3) \end{bmatrix}^T \begin{bmatrix} w_1(\xi) \\ \frac{\partial w_1}{\partial \eta}(\xi) \\ w_2(\xi) \\ \frac{\partial w_2}{\partial \eta}(\xi) \end{bmatrix} . \quad (11)$$

If the above derived relations are substituted in the virtual work balance and if for the virtual displacements $\delta w(\xi,\eta)$ an approximation of the same kind as for the displacements $w(\xi,\eta)$ is chosen, then the internal virtual work can be expressed in scaled boundary coordinates in the following manner:

$$\begin{aligned} \delta W_i \quad = \quad & \int_0^{\Gamma}\int_{\xi_i}^{\xi_e} \left(\left(\frac{1}{\xi^2}\hat{\mathbf{B}}_6\frac{\partial}{\partial\eta} + \hat{\mathbf{B}}_7\frac{\partial}{\partial\xi^2} + \frac{1}{\xi^2}\hat{\mathbf{B}}_8\frac{\partial^2}{\partial\eta^2} \right.\right. \\ & \left.\left. + \frac{1}{\xi}\hat{\mathbf{B}}_9\frac{\partial^2}{\partial\xi\partial\eta} \right)\mathbf{N}_w\delta\mathbf{w}_h \right)^T \mathbf{D}_D \\ & \left(\left(\frac{1}{\xi^2}\hat{\mathbf{B}}_6\frac{\partial}{\partial\eta} + \hat{\mathbf{B}}_7\frac{\partial}{\partial\xi^2} + \frac{1}{\xi^2}\hat{\mathbf{B}}_8\frac{\partial^2}{\partial\eta^2} \right.\right. \\ & \left.\left. + \frac{1}{\xi}\hat{\mathbf{B}}_9\frac{\partial^2}{\partial\xi\partial\eta} \right)\mathbf{N}_w\mathbf{w}_h \right) \xi \mathrm{det}\mathbf{J}^* d\xi d\eta \, . \end{aligned} \quad (12)$$

For the sake of simplicity, the following abbreviations are introduced:

$$\begin{aligned} &\mathbf{B}_{6w}(\tilde{\eta}) = \hat{\mathbf{B}}_6\mathbf{N}_{w,\eta}(\tilde{\eta}), \qquad &&\mathbf{B}_{7w}(\tilde{\eta}) = \hat{\mathbf{B}}_7\mathbf{N}_w(\tilde{\eta}), \\ &\mathbf{B}_{8w}(\tilde{\eta}) = \hat{\mathbf{B}}_8\mathbf{N}_{w,\eta\eta}(\tilde{\eta}), \qquad &&\mathbf{B}_{9w}(\tilde{\eta}) = \hat{\mathbf{B}}_9\mathbf{N}_{w,\eta}(\tilde{\eta}). \end{aligned} \quad (13)$$

The integrals along the boundary are computed numerically in an element-wise manner. Finally, they are assembled for the entire domain in the same way as the element stiffness matrix in the standard finite element method. For clearness, the integrals along the discretised boundary are posed, introducing the following coefficient matrices:

$$\begin{aligned} \mathbf{E}_0 &= \int_0^{\Gamma} \mathbf{B}_{7w}^T\mathbf{D}_D\mathbf{B}_{7w}\mathrm{det}\mathbf{J}^* d\eta \, , \\ \mathbf{E}_1 &= \int_0^{\Gamma} \mathbf{B}_{7w}^T\mathbf{D}_D\mathbf{B}_{9w}\mathrm{det}\mathbf{J}^* d\eta \, , \\ \mathbf{E}_2 &= \int_0^{\Gamma} \mathbf{B}_{7w}^T\mathbf{D}_D\left(\mathbf{B}_{6w}+\mathbf{B}_{8w}\right)\mathrm{det}\mathbf{J}^* d\eta \, , \\ \mathbf{E}_3 &= \int_0^{\Gamma} \mathbf{B}_{9w}^T\mathbf{D}_D\mathbf{B}_{9w}\mathrm{det}\mathbf{J}^* d\eta \, , \\ \mathbf{E}_4 &= \int_0^{\Gamma} \mathbf{B}_{9w}^T\mathbf{D}_D\left(\mathbf{B}_{6w}+\mathbf{B}_{8w}\right)\mathrm{det}\mathbf{J}^* d\eta \, , \\ \mathbf{E}_5 &= \int_0^{\Gamma} \left(\mathbf{B}_{6w}+\mathbf{B}_{8w}\right)^T\mathbf{D}_D\left(\mathbf{B}_{6w}+\mathbf{B}_{8w}\right)\mathrm{det}\mathbf{J}^* d\eta \, . \end{aligned} \quad (14)$$

Afterwards, the internal work is integrated by parts twice with respect to ξ. Finally, the following expression is obtained for the internal virtual work:

$$\begin{aligned} \delta W_i = \int_{\xi_i}^{\xi_e} & \delta\mathbf{w}_h^T \left[\mathbf{E}_0\xi\mathbf{w}_{h,\xi\xi\xi\xi} + \left(2\mathbf{E}_0+\mathbf{E}_1-\mathbf{E}_1^T\right)\mathbf{w}_{h,\xi\xi\xi} \right. \\ & + \left(\mathbf{E}_2+\mathbf{E}_2^T-\mathbf{E}_3\right)\frac{1}{\xi}\mathbf{w}_{h,\xi\xi} \\ & + \left(-2\mathbf{E}_2+\mathbf{E}_3-\mathbf{E}_4+\mathbf{E}_4^T\right)\frac{1}{\xi^2}\mathbf{w}_{h,\xi} \\ & \left. + \left(2\mathbf{E}_2+2\mathbf{E}_4+\mathbf{E}_5\right)\frac{1}{\xi^3}\mathbf{w}_h \right] d\xi \\ + & \left[\delta\mathbf{w}_{h,\xi}^T \left[\xi\mathbf{E}_0\mathbf{w}_{h,\xi\xi} + \mathbf{E}_1\mathbf{w}_{h,\xi} + \frac{1}{\xi}\mathbf{E}_2\mathbf{w}_h \right] \right]_{\xi_i}^{\xi_e} \\ + & \left[\delta\mathbf{w}_h^T \left[-\xi\mathbf{E}_0\mathbf{w}_{h,\xi\xi\xi} + \left(-\mathbf{E}_0-\mathbf{E}_1+\mathbf{E}_1^T\right)\mathbf{w}_{h,\xi\xi} \right. \right. \\ & \left. \left. + \frac{1}{\xi}\left(-\mathbf{E}_2+\mathbf{E}_3\right)\mathbf{w}_{h,\xi} + \frac{1}{\xi^2}\left(\mathbf{E}_2+\mathbf{E}_4\right)\mathbf{w}_h \right] \right]_{\xi_i}^{\xi_e} . \end{aligned} \quad (15)$$

According to the virtual work equivalence, the integrand in the integral of Eqn. (15) must vanish for arbitrary virtual displacements. Additionally, the terms of the internal virtual work, which have to be evaluated at the boundaries ξ_e, ξ_i, have to correspond to the work of the external nodal forces and moments. So, all of the three following conditions must be satisfied:

$$\begin{aligned} & \mathbf{E}_0\xi^4\mathbf{w}_{h,\xi\xi\xi\xi}(\xi) + \left[2\mathbf{E}_0+\mathbf{E}_1-\mathbf{E}_1^T\right]\xi^3\mathbf{w}_{h,\xi\xi\xi}(\xi) \\ & + \left[\mathbf{E}_2+\mathbf{E}_2^T-\mathbf{E}_3\right]\xi^2\mathbf{w}_{h,\xi\xi}(\xi) \\ & + \left[-2\mathbf{E}_2+\mathbf{E}_3-\mathbf{E}_4+\mathbf{E}_4^T\right]\xi\mathbf{w}_{h,\xi}(\xi) \\ & + \left[2\mathbf{E}_2+2\mathbf{E}_4+\mathbf{E}_5\right]\mathbf{w}_h(\xi) = 0 \, , \end{aligned} \quad (16)$$

$$-\mathbf{E}_w(\xi_i)\begin{bmatrix} \mathbf{w}_{h,\xi\xi\xi}(\xi_i) \\ \mathbf{w}_{h,\xi\xi}(\xi_i) \\ \mathbf{w}_{h,\xi}(\xi_i) \\ \mathbf{w}_h(\xi_i) \end{bmatrix} = \begin{bmatrix} \mathbf{f}(\xi_i) \\ \mathbf{m}(\xi_i) \end{bmatrix} , \quad (17)$$

$$\mathbf{E}_w(\xi_e)\begin{bmatrix} \mathbf{w}_{h,\xi\xi\xi}(\xi_e) \\ \mathbf{w}_{h,\xi\xi}(\xi_e) \\ \mathbf{w}_{h,\xi}(\xi_e) \\ \mathbf{w}_h(\xi_e) \end{bmatrix} = \begin{bmatrix} \mathbf{f}(\xi_e) \\ \mathbf{m}(\xi_e) \end{bmatrix} . \quad (18)$$

For convenience, in the above posed equations the following abbreviation is used

$$\mathbf{E}_w = \begin{bmatrix} -\xi\mathbf{E}_0 & -\mathbf{E}_0-\mathbf{E}_1+\mathbf{E}_1^T & \frac{1}{\xi}\left(-\mathbf{E}_2+\mathbf{E}_3\right) & \frac{1}{\xi^2}\left(\mathbf{E}_2+\mathbf{E}_4\right) \\ 0 & \xi\mathbf{E}_0 & \mathbf{E}_1 & \frac{1}{\xi}\mathbf{E}_2 \end{bmatrix} . \quad (19)$$

Eqn. (16) is the so-called scaled boundary equation in displacements. Obviously, the governing equations have been weakened in the boundary direction in a finite element manner, but still remain strong in scaling direction.

3.3. Solution procedure

Using an ansatz of the form

$$\mathbf{w}_h(\xi) = c_1\xi^{\lambda_1}\boldsymbol{\psi}_1 + c_2\xi^{\lambda_2}\boldsymbol{\psi}_2 + ... + c_n\xi^{\lambda_n}\boldsymbol{\psi}_n \quad (20)$$

for the homogeneous set of Euler-Cauchy differential equations, given by Eqn. (16), an eigenvalue problem of fourth order is ob-

tained:

$$\Big[\lambda^4\mathbf{E}_0+\lambda^3\left(-4\mathbf{E}_0+\mathbf{E}_1-\mathbf{E}_1^T\right) +\lambda^2\left(5\mathbf{E}_0-3\mathbf{E}_1+3\mathbf{E}_1^T+\mathbf{E}_2+\mathbf{E}_2^T-\mathbf{E}_3\right) +\lambda\left(-2\mathbf{E}_0+2\mathbf{E}_1-2\mathbf{E}_1^T-3\mathbf{E}_2-\mathbf{E}_2^T+2\mathbf{E}_3-\mathbf{E}_4+\mathbf{E}_4^T\right) +(2\mathbf{E}_2+2\mathbf{E}_4+\mathbf{E}_5)\Big]\boldsymbol{\psi}=\mathbf{0}. \tag{21}$$

This eigenvalue problem can be solved by an eigenvalue decomposition. The general solution to the homogeneous set of Euler-Cauchy differential equations, given by Eqn. (16), can be posed in the following form:

$$\begin{aligned}\mathbf{w}_h &= \Big[\boldsymbol{\Psi}^I\lceil\xi^{\alpha_k}\cos(\beta_k\ln\xi)+\gamma\xi^{\alpha_k}\sin(\beta_k\ln\xi)\rfloor \\ &\quad+\boldsymbol{\Psi}^{II}\lceil\ln(\xi)\,\xi^{\alpha_k}\cos(\beta_k\ln\xi)+\gamma\ln(\xi)\,\xi^{\alpha_k}\sin(\beta_k\ln\xi)\rfloor\Big]\mathbf{c}_k \\ &= \mathbf{F}_w(\xi)\mathbf{c}_k\end{aligned} \tag{22}$$

Where the $\lambda_k=\alpha_k+i\beta_k$ represent pairs of conjugate-complex eigenvalues, $\gamma=1\vee\gamma=-1$ depending whether the imaginary part of the corresponding eingenvalue is positive or negative. $\boldsymbol{\Psi}^I$ and $\boldsymbol{\Psi}^{II}$ are matrices, containing the corresponding eigenvectors and generalized eigenvectors, whereas generalized eigenvectors have to be determined by an additional Jordan transformation. Each exponent λ_k and its corresponding eigenvector $\boldsymbol{\psi}_k$ can be interpreted as an independent deformation mode. The constants $\mathbf{c}_k$ reflect the weightings of the corresponding deformation modes due to boundary conditions. Kinematic boundary conditions are given by

$$\begin{aligned}\mathbf{w}_i &= \mathbf{N}_w\mathbf{F}_w(\xi_i)\mathbf{c}_k\ , \\ \boldsymbol{\phi}_i &= -\left(\hat{\mathbf{B}}_3\mathbf{N}_w\mathbf{F}_{w,\xi}(\xi_i)+\frac{1}{\xi_i}\hat{\mathbf{B}}_4\mathbf{N}_{w,\eta}\mathbf{F}_w(\xi_i)\right)\mathbf{c}_k\ , \\ \mathbf{w}_e &= \mathbf{N}_w\mathbf{F}_w(\xi_e)\mathbf{c}_k\ , \\ \boldsymbol{\phi}_e &= -\left(\hat{\mathbf{B}}_3\mathbf{N}_w\mathbf{F}_{w,\xi}(\xi_e)+\frac{1}{\xi_e}\hat{\mathbf{B}}_4\mathbf{N}_{w,\eta}\mathbf{F}_w(\xi_e)\right)\mathbf{c}_k\ .\end{aligned} \tag{23}$$

Solving these equations for the unknown constants

$$\mathbf{c}_k=\mathbf{F}_c^{-1}\begin{bmatrix}\mathbf{w}_i\\ \boldsymbol{\phi}_i\\ \mathbf{w}_e\\ \boldsymbol{\phi}_e\end{bmatrix} \tag{24}$$

and substituting these relations in Eqns. (17) and (18), then the equlibrium requirement is finally reduced to the form:

$$\begin{bmatrix}\mathbf{f}_i\\ \mathbf{m}_i\\ \mathbf{f}_e\\ \mathbf{m}_e\end{bmatrix}=\mathbf{K}\begin{bmatrix}\mathbf{w}_i\\ \boldsymbol{\phi}_i\\ \mathbf{w}_e\\ \boldsymbol{\phi}_e\end{bmatrix}\ . \tag{25}$$

Herein, $\mathbf{K}$ describes the element stiffness matrix of the domain:

$$\mathbf{K}=\begin{bmatrix}-\mathbf{E}_w(\xi_i)\begin{bmatrix}\mathbf{F}_{w,\xi\xi\xi}(\xi_i)\\ \mathbf{F}_{w,\xi\xi}(\xi_i)\\ \mathbf{F}_{w,\xi}(\xi_i)\\ \mathbf{F}_w(\xi_i)\end{bmatrix}\\ \mathbf{E}_w(\xi_e)\begin{bmatrix}\mathbf{F}_{w,\xi\xi\xi}(\xi_e)\\ \mathbf{F}_{w,\xi\xi}(\xi_e)\\ \mathbf{F}_{w,\xi}(\xi_e)\\ \mathbf{F}_w(\xi_e)\end{bmatrix}\end{bmatrix}\mathbf{F}_c^{-1}\ . \tag{26}$$

Boundary conditions pose constraints at subsets of the nodal displacements $\mathbf{w}_i,\mathbf{w}_e$ and the nodal rotations $\boldsymbol{\phi}_i,\boldsymbol{\phi}_e$. In the element stiffness matrix, these conditions are assembled in the same manner as in the stiffness matrix of the standard finite element method. If the displacements at the boundaries are determined, the constants $\mathbf{c}_k$ can be calculated using Eqn. (24). Finally, the displacement field all over the domain can be expanded using Eqn. (22).

3.4. Enhancements of C_1 conform formulations for the displacements at discretised boundaries including corners

For discretised boundaries, including corners, the approximation of the displacement field as described in section 3.2 does not satisfy C_1 continuity requirements, because the derivation $\frac{\partial w}{\partial\eta}$ can not be specified uniquely along the corner line of two adjacent elements, compare to Fig. 3. The way, how the displacements are approximated, must be modified.

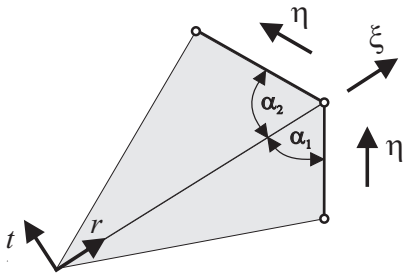

Figure 3: Scaled boundary discretisation at corners.

Therefore, an additional local Cartesian coordinate system(r,t), as depicted in Fig. 3, is introduced at the scaling centre. The r-coordinate runs from the scaling centre to the corner, the other coordinate t is orthogonal to the boundary of two adjacent elements including a corner. In order to ensure C_1 contiuity for the regarded case, the displacement w and its deflections $\frac{\partial w}{\partial r}$ and $\frac{\partial w}{\partial t}$ have to proceed continously along the boundaries of the adjacent elements. If these continuity requirements are posed in scaled boundary coordinates, the following relation for the deflection $\frac{\partial w}{\partial t}$ at the corner can be derived.

$$\frac{\partial w^C}{\partial t}(\xi)=\xi T w^C_{h,\xi}(\xi) \tag{27}$$

Whereas the coefficient T depends only on the geometry of the corner:

$$T=T(\alpha_1,\alpha_2). \tag{28}$$

If for a corner node the unknown displacement function $\frac{\partial w}{\partial\eta}(\xi)$ is replaced by the relation, given by Eqn. 27, C_1 continuity requirements hold and the displacement field can be approximated for an element containing a corner as follows:

$$w(\xi,\eta)=\mathbf{N}_w(\tilde{\eta})\mathbf{w}_h(\xi)^E+\mathrm{N}_w(\tilde{\eta})w_h^C(\xi)+\xi\bar{\mathrm{N}}_w(\tilde{\eta})Tw^C_{h,\xi}(\xi). \tag{29}$$

The superscripts E and C stand for the displacements of edge respectively corner nodes. Again Hermitian polynomials of cubic order are applied for displacement shape functions. If Eqn. (29) is substituted in the virtual work balance and the integration along the boundary is performed and finally the internal virtual work is integrated twice by parts with respect to ξ, as illustrated more detailed in section 3.2, then finally a set of Euler-Cauchy differential equations of sixth order is obtained for the scaled boundary finite element equation. The solution and the assemblage of the element stiffness matrix proceed in the same manner, as described in the previous section.

4. Examples

In the scaled boundary finite element method, three elemental scaling cases have to be distinguished:

$$\begin{array}{lllll} I: & \xi_i > 0 & \wedge & \xi_e = 1\,, \\ II: & \xi_i = 0 & \wedge & \xi_e = 1\,, \\ III: & \xi_i = 1 & \wedge & \xi_e \to +\infty\,. \end{array} \tag{30}$$

The first and the second scaling case describe bounded media. In the first case, at the inner boundary ($\xi_i > 0$) an additional equivalent set of nodes arises, where static or dynamic boundary conditions have to be prescribed. For the expansion of the solution, the whole spectrum of eigenvalues, which are found by an eigenvalue decomposition of Eqn. (16), must taken into account. In the second case, where ξ runs from the scaling centre ($\xi_i = 0$) to the discretised outer boundary ($\xi_e = 1$), only at the boundary nodal degrees of freedom exist. So, for the composition of the solution an appropriate subset of the n eigenvalues and corresponding generalized eigenvectors must be selected. The conditions for an adequate selection are, that the displacement $w(\xi \to 0)$ and the rotations $\boldsymbol{\phi}(\xi \to 0)$ have to stay finite at the scaling centre. Additionally, the sectional forces and moments have to satisfy regularity conditions at the scaling centre. An unbounded medium is specified by the third scaling case. Due to the relevance in engineering, the focus of this work is on the scaling cases I and II.

4.1. Plate of trapezoidal shape

First of all, a trapezoidal plate, as depicted in Fig. 4, is examined. The scaling coordinate ξ runs from $\xi_i = 0.5$ at the inner boundary to $\xi_e = 1.0$ at the outer boundary.

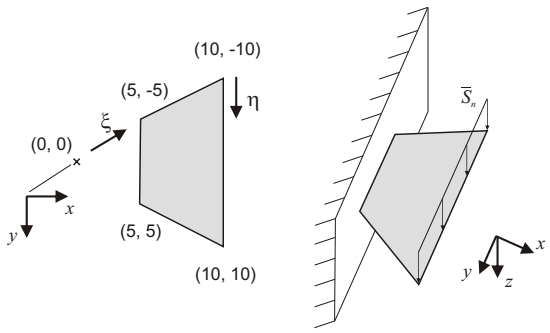

Figure 4: Trapezoidal plate.

The plate's thickness is assumed to be 1mm. For the material data, the values of steel are chosen ($E = 210000^{\mathrm{N}}/_{\mathrm{mm}^2}$, $\nu = 0.3$). The plate is clamped at the inner boundary. The outer boundary is loaded by a transverse shear force $\bar{S} = 10^{\mathrm{N}}/_{\mathrm{mm}}$. The spectrum of the exponents λ_k, which are obtained by an eigenvalue decomposition of Eqn. (21), is shown in Fig. 5 for a discretisation of the trapezoidal plate with ten elements along the outer boundary. The real parts of the eigenvalues are posed on the abszissa, the imaginary parts are posed on the ordinate. The spectrum is symmetric to one, which corresponds to analytical solutions given in (Ref. [10]). The symmetry axis is given as a thin solid line.

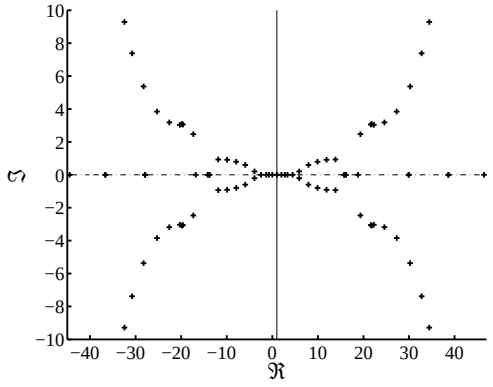

Figure 5: Spectrum of the eigenvalues.

There is only one eigenvalue $\lambda_0 = 0$. The corresponding deformation mode describes a rigid body motion in the thickness direction of the plate. Furthermore, there are four exponents $\lambda_{1,2,3,4} = 1$. Two of them describe rotations around the x- and y-axis. Moreover, there is one exponent $\lambda_5 = 2$, which can be identified as a constant curvature state. The proper account of rigid body modes and constant curvature states is a necessary requirement for the convergence of plate bending elements.
A convergence study has been undertaken to validate the results. In Fig. 6, the maximum displacement w, which is found at the edge of the outer boundary, is presented for different numbers of elements.

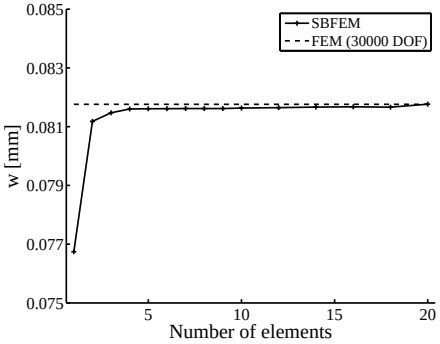

Figure 6: Max. displacements for different discretisations.

As reference acts a displacement, which was determined by a finite element analysis with ABAQUS using triangular STRI3 elements, based on pure Kirchhoff kinematics. For the FE-analysis a very fine discretisation (30000 DOF) was applied, which converged. As can be seen from Fig. 6 , the solution of the SBFEM converges rapidly. For a discretisation with four elements, respectively fourty degrees of freedom, the relative error is already smaller than 0.2%.
In Fig. 7 the displacements w along the outer boundary ($x = 10$mm) are shown. For the calculation of the displacement field with the SBFEM, the outer boundary was discretised using twenty line elements.

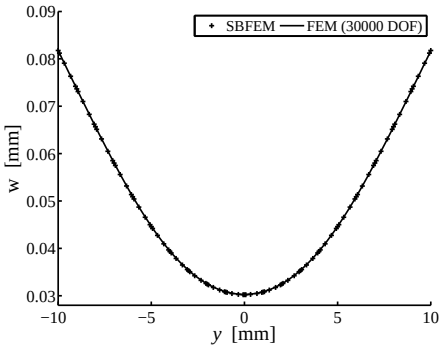

Figure 7: Displacements w along the boundary ($x = 10$mm).

As can be seen from Fig. 7, the SBFEM provides a fine approximation for the displacements at the boundary, compared to the displacements of the reference FEM solution, whereas the discretisation effort using the SBFEM is much smaller than that of the FEM. In Fig. 8, the displacements w along the upper boundary of the trapezoidal plate in scaling direction are depicted. In scaling direction, the SBFEM provides a solution in analytical form. Even though a very rough discretisation of the boundary is used, the SBFEM retains in contrast to the standard FEM a very precise approximation in scaling direction.

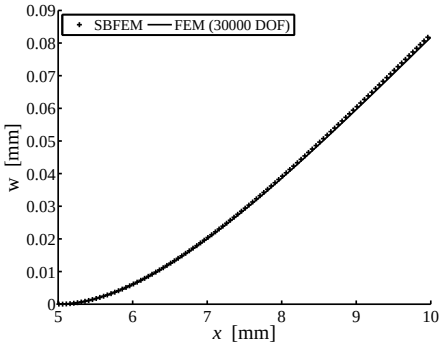

Figure 8: Displacements w at the upper boundary in ξ-direction.

4.2. Triangular Plate

As second example, a triangular plate, as pictured in Fig. 9, is analysed. For the material data and the plate's thickness, the same assumptions as before for the plate with trapezoidal shape are made. The plate is loaded by a distributed moment, which varies linearly along the boundary $\bar{M}_n = (-10 + \eta)$N.

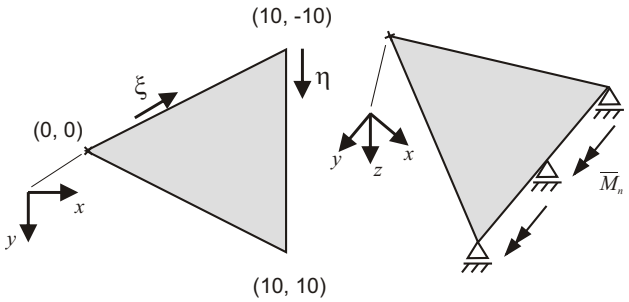

Figure 9: Triangular plate.

At the corners and at the middle of the boundary $x = 10$mm, brackets hold lateral forces. Additionally, rotations around the y-axis are prevented by a bearing at the midpoint of the outer boundary ($x = 10$mm). For the triangular plate, the scaling coordinate ξ runs from the scaling centre ($\xi_0 = 0$) to the boundary ($\xi_e = 1$). So, the triangular plate stands for scaling case II. For the expansion of the solution, an appropriate subset of the n displacement modes must be chosen. The criteria for the selection have been specified more detailed in the former context.

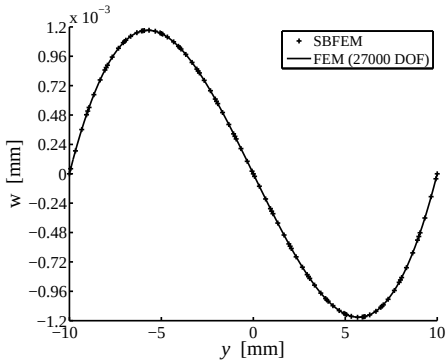

Figure 10: Displacements w along the boundary ($x = 10$mm).

In Fig. 10, the displacements of the SBFEM are compared to reference displacements, which were determined by a FE-analysis using ABAQUS STRI3 elements (27000 DOF). As seen before, the new formulation of the SBFEM to plate bending problems provides an excellent approximation. Finally, the displacements in scaling direction at the upper boundary of the trinangular plate are compared to the displacements of the FEM reference solution.

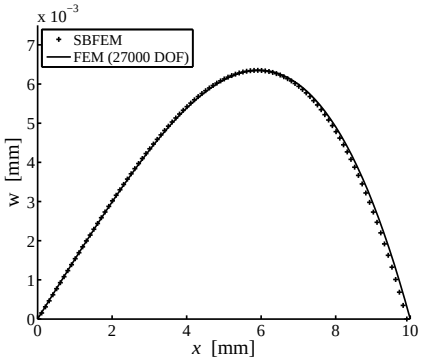

Figure 11: Displacements w at the upper boundary in ξ-direction.

The displacements of the FEM reference solution and those, which were determined using the SBFEM, also show a good agreement.

5. Conclusions

The scaled boundary finite-element method has been extended successfully to plate bending problems. The semi-analytical approximation reduces the number of the degrees of freedom, but still retains a high quality of approximation. Due to the expansion in scaling direction, field exponents are calculated efficiently, making the method especially useful for the application to notch and crack problems, where singularities may occur.

References

[1] Wolf, J. P. and Song, C., *Finite-Element Modelling of unbounded Media*, Wiley, Chichester, 1996.

[2] Wolf, J. P. and Song, C. The scaled boundary finite-element method - a primer: Derivations, *Computers and Structures*, 78, pp. 191 - 210, 2000.

[3] Wolf, J. P. and Song, C. The scaled boundary finite-element method - a primer: Solution procedures, *Computers and Structures*, 78, pp. 211 - 225, 2000.

[4] Deeks, A. J. and Wolf, J. P., A virtual work derivation of the scaled boundary finite-element method for elastostatics, *Computational Mechanics*, 28, pp. 489 - 504, 2002.

[5] Song, C., Evaluation of power-logarithmic singularities, T-stresses and higher order terms of in-plane singular stress fields at cracks and multi-material corners, *Engineering Fracture Mechanics*, 72, pp. 1498 - 1530, 2005.

[6] Song, C. and Vrcelj, Z. Evaluation of dynamic stress intensity factors and T-sress using the scaled boundary finite-element method, *Engineering Fracture Mechanics*, 72, pp. 1498 - 1530, 2005.

[7] Lindemann, J. and Becker, W., Free-edge stresses around holes in laminates by the boundary finite-element method, *Mech. Comp. Mat.*, 38, pp. 407 - 416, 2002.

[8] Artel, J. and Becker, W., On kinematic coupling equations within the scaled boundary finite-element method, *Arch. Appl. Mech.*, 76, pp. 617 - 633, 2006.

[9] Zienkiewicz, O.C. and Taylor, R.L., *The Finite Element Method for Solid and Structural Mechanics*, sixth ed., Butterworth-Heinemann, Oxford, 2005.

[10] Timoshenko , S., *Theory of Plates and Shells*, sixth ed., McGRAW-HILL BOOK COMPANY , New York, 1940.